THE JOURNAL OF PHYSICAL CHEMISTRY C

Article

Cite This: J. Phys. Chem. C 2018, 122, 4731−4736

pubs.acs.org/JPCC

Iron Superhydrides FeH_5 and FeH_6: Stability, Electronic Properties, and Superconductivity

Alexander G. Kvashnin,*[†,‡] Ivan A. Kruglov,[‡,§] Dmitrii V. Semenok,[†,‡] and Artem R. Oganov[†,‡,§,∥]

[†]Skolkovo Institute of Science and Technology, Skolkovo Innovation Center, 3 Nobel Street, 143026 Moscow, Russian Federation

[‡]Moscow Institute of Physics and Technology, 9 Institutsky Lane, 141700 Dolgoprudny, Russian Federation

[§]Dukhov Research Institute of Automatics (VNIIA), Moscow 127055, Russian Federation

[∥]International Center for Materials Discovery, Northwestern Polytechnical University, Xi'an 710072, China

Supporting Information

ABSTRACT: Recently, a large number of works devoted to the search for new hydrides with record high-temperature superconductivity and at the same time the successful synthesis of potential high-T_C superconducting FeH_5 were reported. We present a systematic search for stable compounds in the Fe−H system using the variable-composition version of the evolutionary algorithm USPEX. All known (FeH, FeH_3, FeH_5) and several new (Fe_3H_5, Fe_3H_{13}, and FeH_6) iron hydrides were found to be stable, resulting in a very complex phase diagram with rich structural relationships between phases. We calculate electronic properties of two potentially high-T_C FeH_5 and FeH_6 phases in the pressure range from 150 to 300 GPa. Indeed, hydrogen-rich FeH_5 and FeH_6 phases were found to be superconducting within Bardeen−Cooper−Schrieffer theory, with T_C values of up to 46 K.

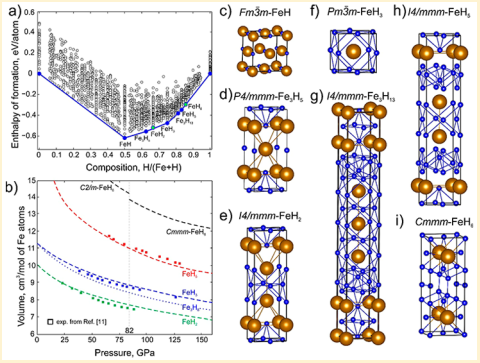

INTRODUCTION

Theoretical searches for new iron hydrides have attracted the attention of the scientific community since the 1970s when the phase transitions in the Fe−H system were first experimentally investigated under pressure.[1,2] At atmospheric pressure, there are no stable solid iron hydrides, but there is substantial solubility of hydrogen in iron.[3,4] However, molecules such as FeH, FeH_2, Fe_2H_4, and molecular complexes, namely $FeH_2(H_2)_2$, $FeH{\cdot}H_2$, and $FeH_2(H_2)_3$, were identified using infrared spectroscopy at low temperatures in an inert gas matrix.[5−7] The FeH phase was known as the only one in the Fe−H system for a long time, until new stable iron hydrides were theoretically predicted in 2012 by Bazhanova et al.[8] using the evolutionary algorithm USPEX with fixed-composition searches (at that time probing only compositions FeH, FeH_2, FeH_3, and FeH_4). New FeH_3 and FeH_4 phases were predicted to be stable in calculations done at 100 GPa[8] with evidence for likely stability of FeH_2 at lower pressures. Recently structures of FeH_4 under pressure were studied by another group.[9] In 2014, Pépin et al.[10] experimentally synthesized the earlier predicted FeH_3 at 86 GPa. Besides the FeH_3 phase another new iron hydride ($FeH_{\sim 2}$) was experimentally found.[10] Recent experimental investigation by Pépin et al.[11] reported synthesis of FeH_5 at pressures above 130 GPa. Its crystal structure was partially determined using available XRD data, but the exact positions of hydrogen atoms were identified using DFT calculations.[3]

Recent exceptional surge of interest in hydrides is due to the experimental and (mostly) theoretical findings of high-T_C superconductivity under high pressures, e.g., refs 12−20. Moreover, recent theoretical investigation of new hydrides in the Ge−H[21] ($T_C \sim 60$ K), Sn−H[19] ($T_C \sim 100$), $MgGeH_6$[22] ($T_C \sim 132$ K), and H−S[14] ($T_C \sim 200$ K) systems and in Th−H[23] and U−H[20] systems ($T_C \sim 194$ K) at high pressures as well as landmark achievements in experimental synthesis of H_3S[17] ($T_C \sim 203$ K), PH_3[24] ($T_C \sim 100$ K), and Si_2H_6[25] ($T_C \sim 76$ K) has inspired exploration of new hydrides. Fresh theoretical work by Majumdar et al.[26] predicted a relatively high T_C (~51 K) at 130 GPa for FeH_5. All these findings motivate us to study in detail the Fe−H system, in particular stability and superconducting properties of new phases.

Iron is a distinctive element for superconductivity. It was assumed for a long time that magnetism of iron makes superconductivity impossible. However, in 2001 non-phonon-mediated superconductivity was discovered in nonmagnetic ε-Fe with $T_C \sim 2.3$ K at 15 GPa.[27−29]

Since the unexpected discovery of iron-containing superconducting pnictides in 2008 with potential upper critical magnetic fields of up to 200 T,[30,31] different mechanisms of superconductivity in such materials in relation with magnetism are still under discussion.[32] In this case special interest to FeH_5 is caused by the fact that it is the first synthesized superhydride of iron, where superconductivity could come from both electron−phonon coupling and magneto−elastic coupling in

Received: February 6, 2018
Published: February 6, 2018

DOI: 10.1021/acs.jpcc.8b01270
J. Phys. Chem. C 2018, 122, 4731−4736

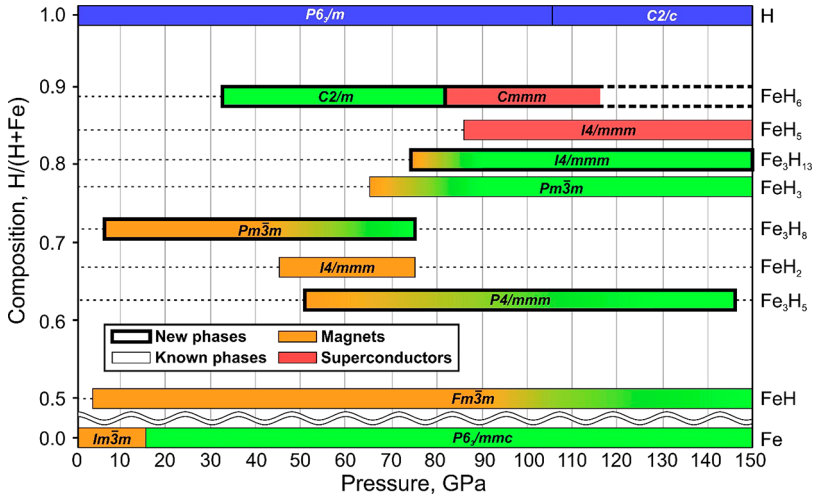

Figure 1. Pressure−composition phase diagram of the Fe−H system. FeH_5 and FeH_6 are metallic and superconducting. All shown phases, except hydrogen allotropes, are metallic.

the spin-driven scenario[33,34] or/and orbital fluctuation pairing.[35,36]

In the last years many developments have been made in order to extend the scope and predictive power of the USPEX code. One of them was the implementation of a variable-composition search,[37] which allows one to explore the whole compositional space in the studied system in a single calculation. These improvements and previous experimental studies of iron hydrides[10,11] motivated us to perform the evolutionary variable-composition search for new phases in the Fe−H system. The detailed investigation of stability, structural, electronic, and superconducting properties of predicted hydrogen-rich phases was carried out, and we estimated the possible contribution of electron−phonon interaction to superconductivity of iron hydrides.

COMPUTATIONAL DETAILS

We performed variable-composition searches for stable compounds in the Fe−H system at pressures of 0, 50, 100, and 150 GPa using the USPEX[39,40,38] package. The first generation (120 structures) was created using a random symmetric generator, while all subsequent generations (100 structures) contained 20% random structures and 80% created using heredity, softmutation, and transmutation operators. Here, evolutionary searches were combined with structure relaxations using density functional theory (DFT)[41,42] within the spin-polarized generalized gradient approximation (Perdew−Burke−Ernzerhof, or PBE functional)[43] and the projector-augmented wave method,[44,45] as implemented in the VASP package.[46−48] The plane wave kinetic energy cutoff was set to 600 eV, and the Brillouin zone was sampled by Γ-centered k-point meshes with resolution $2\pi \times 0.05$ Å^{-1}.

By definition, a thermodynamically stable phase has the lowest Gibbs free energy (or, at 0 K, lowest enthalpy) among any phase or phase assemblage of the same composition. Thermodynamic convex hull construction compactly presents information about all possible formation and decomposition reactions; phases that are located on the convex hull are stable at given pressure. Stable structures of elemental Fe and H were taken from USPEX calculations and from refs 49−51 and 52, respectively.

Calculations of superconducting T_C were carried out using the QUANTUM ESPRESSO package.[53] Phonon frequencies and electron−phonon coupling (EPC) coefficients were computed using density-functional perturbation theory,[54] employing the plane-wave pseudopotential method and PBE exchange-correlation functional.[43] Convergence tests showed that 70 Ry is a suitable kinetic energy cutoff for the plane-wave basis set. In our calculations of the electron−phonon coupling (EPC) parameter λ, the first Brillouin zone was sampled using $4 \times 4 \times 1$ and $4 \times 4 \times 2$ q-point mesh and a denser $16 \times 16 \times 4$ and $16 \times 16 \times 8$ k-point mesh for FeH_5 and FeH_6, respectively (with Gaussian smearing and $\sigma = 0.05$ Ry), which approximates the zero-width limits in the calculation of λ.

Electronic band structures of FeH_5 and FeH_6 were calculated using both VASP and QE and demonstrated good consistency. Comparison of the phonon densities of states calculated using the finite displacement method (VASP and PHONOPY[55,56]) and density-functional perturbation theory (QE) showed excellent agreement between these methods.

The superconducting transition temperature T_C was estimated by using two equations: "full" Allen−Dynes and "short" modified McMillan equations.[57] The "full" Allen−Dynes equation for calculating T_C has the following form[57]

$$T_C = \omega_{\log}\frac{f_1 f_2}{1.2}\exp\left(\frac{-1.04(1+\lambda)}{\lambda - \mu^* - 0.62\lambda\mu^*}\right) \quad (1)$$

while the modified McMillan equation has the form as

$$T_C = \frac{\omega_{\log}}{1.2}\exp\left(\frac{-1.04(1+\lambda)}{\lambda - \mu - 0.62\lambda\mu^*}\right) \quad (2)$$

The EPC constant λ and logarithmic average frequency $\omega_{\log}$ were calculated as

$$\lambda = \int_{\omega_{\min}}^{\omega_{\max}} \frac{2\cdot a^2F(\omega)}{\omega}\mathrm{d}\omega \quad (3)$$

and

$$\omega_{\log} = \exp\left(\frac{2}{\lambda}\int_{\omega_{\min}}^{\omega_{\max}}\frac{\mathrm{d}\omega}{\omega}\alpha^2F(\omega)\ln(\omega)\right) \quad (4)$$

DOI: 10.1021/acs.jpcc.8b01270
J. Phys. Chem. C 2018, 122, 4731−4736

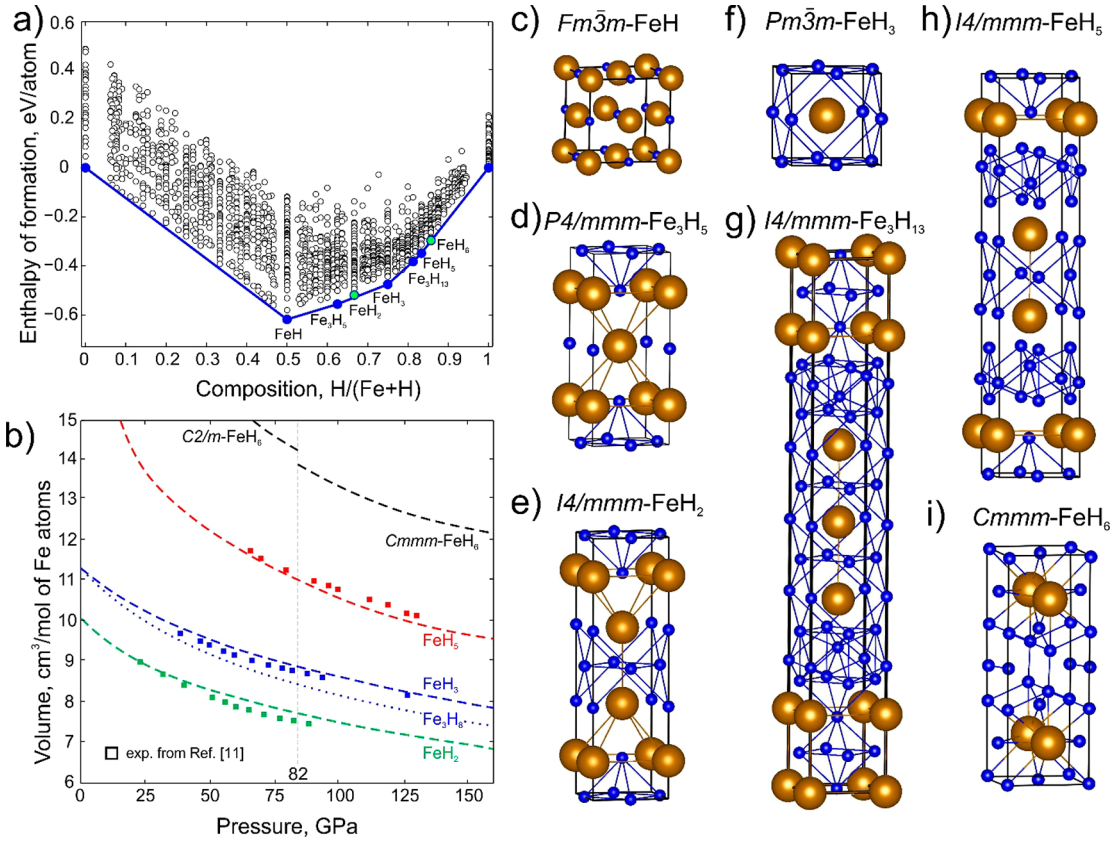

Figure 2. (a) Calculated convex hull of the Fe−H system at 150 GPa. Green points correspond to low-enthalpy metastable FeH_2 and FeH_6. (b) Equations of state of FeH_2, Fe_3H_8, FeH_3, FeH_5, and FeH_6 phases compared with experimental data from ref 11. (c−i) Crystal structures of predicted stable Fe−H phases. Iron atoms are shown by large brown balls and hydrogen atoms by small blue balls. Crystal structures of the predicted phases were generated using VESTA software.[59]

and μ^* is the Coulomb pseudopotential, for which we used widely accepted lower and upper bound values of 0.10 and 0.15.

RESULTS AND DISCUSSION

In order to predict stable phases in the Fe−H system we performed variable-composition evolutionary searches using the USPEX algorithm[39,40,38] in the pressure range from 0 to 150 GPa. A pressure-composition phase diagram was constructed as shown in Figure 1. There are no stable hydride phases in the pressure range from 0 to 5 GPa, which is in agreement with experimental observations.[3,4] Increase of pressure leads to the formation of the $Fm\bar{3}m$-FeH phase which is stable. Another experimentally known phase $I4/mmm$-FeH_2 is magnetic and stable in a relatively narrow pressure range from 45 to 75 GPa, which is in agreement with experiment.[10] This phase was found in experiments at pressures from 67 up to 86 GPa, but was indicated as FeH_2[10] due to undetermined stoicheometry. Our phase diagram (Figure 1) explaind why FeH_2 was not found at higher pressures. New $Pm\bar{3}m$-Fe_3H_8 becomes stable from 5 until 75 GPa. It is important that $Pm\bar{3}m$-Fe_3H_8 is structurally similar to $Pm\bar{3}m$-FeH_3 but with one iron and four hydrogen vacancies in the 2 × 2 × 1 supercell of FeH_3 (see Figure S9 in Supporting Information). At higher pressures it decomposes into the new $P4/mmm$-Fe_3H_5 and $Pm\bar{3}m$-FeH_3. FeH_3 is stable from 65 up to the highest pressure studied here, which agrees with high-pressure experiments where it was synthesized at 86 GPa.[10] The $I4/mmm$-FeH_5 phase recently synthesized[11] at pressures above 130 GPa was found to be thermodynamically stable at pressures from 85 to at least 150 GPa. In the same pressure region we predict new $I4/mmm$-Fe_3H_{13} to be stable. It important that newly predicted Fe_3H_5, Fe_3H_8, and Fe_3H_{13} with compositions close to FeH_2, FeH_3, and FeH_5 display rich polysomatism.[58]

We also found a new hydrogen-rich $C2/m$-FeH_6 phase to be thermodynamically stable at pressures higher than 35 GPa. At ∼82 GPa $C2/m$-FeH_6 transforms to the $Cmmm$-FeH_6 phase (see Figure 1), which remains thermodynamically stable at pressures up to 115 GPa (see Figure S1 in Supporting Information). At pressures between 115 and 150 GPa $Cmmm$-FeH_6 is only 1.5 meV/atom above the decomposition line (see Figure 2a). The magnetic bcc phase of iron transforms to nonmagnetic hcp ε-Fe at 15 GPa (Figure 1) in agreement with experiment, see refs 27−29. Most of the iron hydrides (FeH, Fe_3H_5, Fe_3H_8, FeH_3, and Fe_3H_{13}) are magnetic and become nonmagnetic at high pressures (∼100 GPa). Detailed information on crystal structures of the predicted phases is summarized in Table S1 (see Supporting Information).

Further detailed investigation is devoted to stability, electronic, and superconducting properties of Fe−H phases at 150 GPa.

We built the convex hull for the Fe−H system at 150 GPa (see Figure 2a), which shows that there are five stable Fe−H phases, namely, $Fm\bar{3}m$-FeH, $P4/mmm$-Fe_3H_5, $Pm\bar{3}m$-FeH_3, $Immm$-Fe_3H_{13}, and $I4/mmm$-FeH_5. We found a very large number of phases close to the convex hull. In the iron-rich part of the convex hull (left part of Figure 2a) there is practically a continuum of states very close to decomposition line between Fe and FeH, which corresponds to the formation of solid

DOI: 10.1021/acs.jpcc.8b01270
J. Phys. Chem. C 2018, 122, 4731−4736

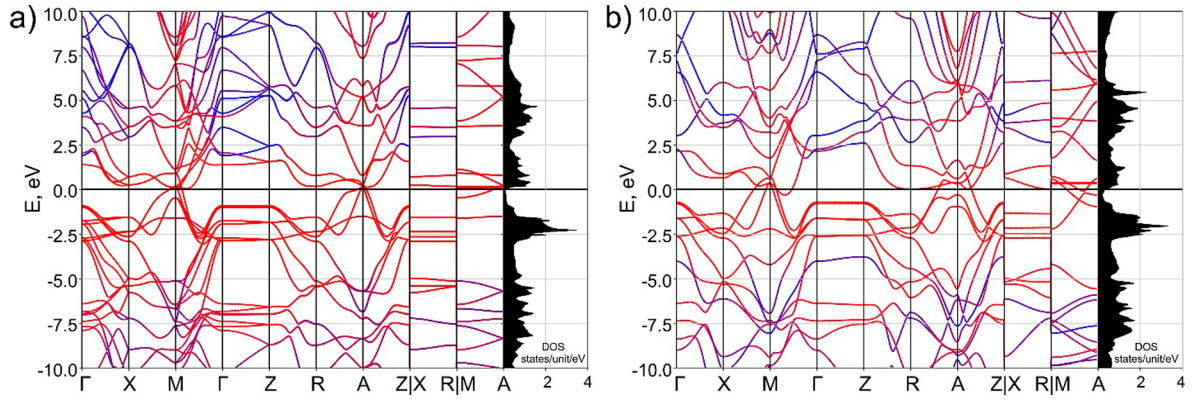

Figure 3. Electronic band structures and densities of states of (a) FeH_5 and (b) FeH_6 at 150 GPa. Red color corresponds to the contribution from Fe, while blue color is for hydrogen atoms.

Table 1. Predicted Superconducting Properties of FeH_5 and FeH_6 Phases[a]

phase	P, GPa	λ	N_f, states/unit/eV	ω_{log}, K	T_C (Allen–Dynes), K	T_C (McMillan), K
FeH_5	150	0.97	0.145	642.3	45.8 (33.6)	42.6 (32.3)
	200	1.05	0.257	492.7	39.7 (30.6)	36.6 (28.8)
	300	1.26	0.318	339.5	35.7 (28.7)	32.2 (26.5)
FeH_6	100	0.37	0.731	973.1	3.9 (1.2)	4.0 (1.2)
	150	0.92	0.436	665.6	42.9 (31.3)	40.2 (29.7)
	300	0.94	0.391	549.6	37.3 (27.6)	34.9 (26.1)

[a] T_C values are given for $\mu^* = 0.1$ (0.15).

solutions of hydrogen in iron in a wide range of concentrations. The hydrogen-rich region (right part of Figure 2a) has almost parabolic convex hull and phases at this region display rich polysomatism.[58] We calculated zero-point energy contribution for all stable iron hydrides at 150 GPa to determine its effect on stability (see Figure S8 in Supporting Information). Addition of the ZPE contribution expands the stability field of *Cmmm*-FeH_6 up to 150 GPa.

Additionally, we calculated equations of state (EOS) of the predicted FeH_2, Fe_3H_8, FeH_3, FeH_5, and FeH_6 phases and compared them with available experimental data from refs 10 and 11 (see Figure 2b). One can see that theory (dashed lines in Figure 2b) agrees very well with experimental data (squares in Figure 2b). EOS of Fe_3H_8 is close to experimental and calculated data for FeH_3 at low pressures (dotted line in Figure 2b). Predicted crystal structures are consistent with all available experimental results. Good agreement with all available experimental data lends confidence to our further predictions that the new FeH_6 hydride (see black dashed line in Figure 2b) should be stable at pressures from 50 GPa (in fact, even lower pressures) to 115 GPa (see Supporting Information).

Crystal structures of FeH, FeH_2, FeH_3, FeH_5, and FeH_6 are shown in Figure 2c–i. FeH has the well-known rocksalt-type structure (see Figure 2c). FeH_2 has orthorhombic structure alternating FeH_3- and FeH-type layers (see Figure S11 in Supporting Information). FeH_3 has a very simple structure (see Figure 2f) in which iron atoms are coordinated by 12 hydrogens; together Fe and H atoms form a cubic close packing. The predicted Fe_3H_{13} phase has layered structure where FeH_3 layers of thickness 4.7 Å (two unit cells of FeH_3) alternate with hydrogen layers. The structure of FeH_5 is similar to Fe_3H_{13} with the only difference in the thickness of FeH_3-type layers which is 2.36 Å (unit cell of FeH_3). Metastable at 150 GPa, the *Cmmm*-FeH_6 phase consists of FeH_3-type layers, similarly to FeH_5, but alternating with thicker hydrogen layers (see Figure 2i) with H_2 molecules (H–H distance 0.74 Å) between the layers. Such layered structure with alternation of hydrogen and FeH_3-type layers is similar to Na_3Cl,[60] which is made of alternating NaCl and Na_2 layers. It is currently unknown why such alternating-layer polysomatic compounds become stable under pressure.

Our main interest here is in hydrogen-rich FeH_5 and FeH_6 and their potential superconductivity in view of recent synthesis and theoretical investigations of various superconducting hydrides.[12−20,24,25] It is important to note that both FeH_5 and FeH_6 remain dynamically stable in the pressure region from 150 to 300 GPa, according to phonon calculations (see Supporting Information Figures S4 and S5).

We have calculated band structures and electronic densities of states of FeH_5 and FeH_6 at 150 GPa (see Figure 3). The atom-projected band structure shows that near the Fermi level the contribution of iron atoms (red color) is dominant. High peaks of the DOS of FeH_5 at −2 eV (see Figure 3a) can be explained by the presence of flat bands in the direction perpendicular to the *c*-axis. Such behavior of the bands indicates a layered structure and weak interaction between layers in FeH_5. All other Fe–H phases are metallic with very low DOS at the Fermi level (<0.15 states/eV/unit).

Similarly, the band structure of FeH_6 shows the presence of flat bands along the high-symmetry c^* direction of the reciprocal space (see Figure 3b). We calculated the electronic DOS for FeH_5 and FeH_6 at pressures of 150, 200, and 300 GPa. The values of the densities of states at the Fermi level are shown in Table 1. One can see that as pressure increases the density of states slightly decreases (see Table 1).

Both Crystal structures and electronic properties of FeH_5 and FeH_6 phases display strong resemblance. We have calculated the electron–phonon coupling (EPC) coefficient λ, ω_{log}, and T_C calculated using both Allen–Dynes and McMillan formulas[57] as a function of pressure (Table 1). One can see

DOI: 10.1021/acs.jpcc.8b01270
J. Phys. Chem. C 2018, 122, 4731−4736

that EPC coefficient of FeH_5 increases with pressure due to increasing density of states N_f (as $\lambda = N_f \times V_{Coulomb}$). At the same time T_C decreases with pressure, due to decreasing ω_{log}. Values of T_C for both phases are reasonably high, ~43−45 K at the pressure of 150 GPa, which is in good agreement with data from ref 26. Below 150 GPa FeH_6 gradually loses its superconducting properties, and below 100 GPa we have not found superconductivity in FeH_6.

CONCLUSIONS

Using the evolutionary crystal structure prediction algorithm USPEX we have uncovered unexpectedly complex chemistry of the Fe−H system in the pressure range from 0 to 150 GPa. We confirmed crystal structures of the experimentally synthesized FeH_2, FeH_3, FeH_5, and predicted new $P4/mmm$-Fe_3H_5, $Immm$-Fe_3H_{13}, $I4/mmm$-FeH_5, and $Cmmm$-FeH_6 phases to be stable at 150 GPa. Many of these phases belong to polysomatic series formed by H-, FeH- and FeH_3 blocks. Predicted crystal structures of hydrogen-rich phases allowed us to perform theoretical calculations of superconducting properties within BCS theory. We showed that both FeH_5 and FeH_6 demonstrate electronic behavior corresponding to two-dimensional metals. T_C values for both $I4/mmm$-FeH_5 and $Cmmm$-FeH_6 do not exceed 46 K at 150 GPa, and decrease with pressure.

ASSOCIATED CONTENT

Supporting Information

The Supporting Information is available free of charge on the ACS Publications website at DOI: 10.1021/acs.jpcc.8b01270.

Crystal data of Fe-H phases, equations for calculation T_C, stability ranges of new iron polyhydrides, crystal structures of FeH, FeH_2, FeH_3, and Fe_3H_8 phases, electronic properties of Fe-H phases, Eliashberg spectral functions for FeH_5 and FeH_6 phases at different pressures, and additional references (PDF)

AUTHOR INFORMATION

Corresponding Author

*E-mail: a.kvashnin@skoltech.ru.

ORCID

Alexander G. Kvashnin: 0000-0002-0718-6691

Notes

The authors declare no competing financial interest.

ACKNOWLEDGMENTS

The work was supported by the Russian Science Foundation (No. 16-13-10459). Calculations were performed on Rurik supercomputer at MIPT.

REFERENCES

(1) Stevenson, D. J. Hydrogen in the Earth's Core. *Nature* **1977**, *268* (5616), 130−131.

(2) Wohlfarth, E. P. The Possibility That ϵ-Fe Is a Low Temperature Superconductor. *Phys. Lett. A* **1979**, *75* (1), 141−143.

(3) Armbruster, M. H. The Solubility of Hydrogen at Low Pressure in Iron, Nickel and Certain Steels at 400 to 600°. *J. Am. Chem. Soc.* **1943**, *65* (6), 1043−1054.

(4) Da Silva, J. R. G.; Mclellan, R. B. The Solubility of Hydrogen in Super-Pure-Iron Single Crystals. *J. Less-Common Met.* **1976**, *50* (1), 1−5.

(5) Chertihin, G. V.; Andrews, L. Infrared Spectra of FeH, FeH_2, and FeH_3 in Solid Argon. *J. Phys. Chem.* **1995**, *99* (32), 12131−12134.

(6) Körsgen, H.; Mürtz, P.; Lipus, K.; Urban, W.; Towle, J. P.; Brown, J. M. The Identification of the FeH_2 Radical in the Gas Phase by Infrared Spectroscopy. *J. Chem. Phys.* **1996**, *104* (12), 4859−4861.

(7) Wang, X.; Andrews, L. Infrared Spectra and Theoretical Calculations for Fe, Ru, and Os Metal Hydrides and Dihydrogen Complexes. *J. Phys. Chem. A* **2009**, *113* (3), 551−563.

(8) Bazhanova, Z. G.; Oganov, A. R.; Gianola, O. Fe−C and Fe−H Systems at Pressures of the Earth's Inner Core. *Phys.-Usp.* **2012**, *55* (5), 489.

(9) Li, F.; Wang, D.; Du, H.; Zhou, D.; Ma, Y.; Liu, Y. Structural Evolution of FeH_4 under High Pressure. *RSC Adv.* **2017**, *7* (21), 12570−12575.

(10) Pépin, C. M.; Dewaele, A.; Geneste, G.; Loubeyre, P.; Mezouar, M. New Iron Hydrides under High Pressure. *Phys. Rev. Lett.* **2014**, *113* (26), 265504.

(11) Pépin, C. M.; Geneste, G.; Dewaele, A.; Mezouar, M.; Loubeyre, P. Synthesis of FeH_5: A Layered Structure with Atomic Hydrogen Slabs. *Science* **2017**, *357* (6349), 382−385.

(12) Gao, G.; Oganov, A. R.; Bergara, A.; Martinez-Canales, M.; Cui, T.; Iitaka, T.; Ma, Y.; Zou, G. Superconducting High Pressure Phase of Germane. *Phys. Rev. Lett.* **2008**, *101* (10), 107002.

(13) Gao, G.; Oganov, A. R.; Li, P.; Li, Z.; Wang, H.; Cui, T.; Ma, Y.; Bergara, A.; Lyakhov, A. O.; Iitaka, T.; et al. High-Pressure Crystal Structures and Superconductivity of Stannane (SnH_4). *Proc. Natl. Acad. Sci. U. S. A.* **2010**, *107* (4), 1317−1320.

(14) Duan, D.; Liu, Y.; Tian, F.; Li, D.; Huang, X.; Zhao, Z.; Yu, H.; Liu, B.; Tian, W.; Cui, T. Pressure-Induced Metallization of Dense $(H_2S)_2H_2$ with High-T_C Superconductivity. *Sci. Rep.* **2015**, *4*, 6968.

(15) Hou, P.; Zhao, X.; Tian, F.; Li, D.; Duan, D.; Zhao, Z.; Chu, B.; Liu, B.; Cui, T. High Pressure Structures and Superconductivity of $AlH_3(H_2)$ Predicted by First Principles. *RSC Adv.* **2015**, *5* (7), 5096−5101.

(16) Li, Y.; Hao, J.; Liu, H.; Tse, J. S.; Wang, Y.; Ma, Y. Pressure-Stabilized Superconductive Yttrium Hydrides. *Sci. Rep.* **2015**, *5*, 09948.

(17) Drozdov, A. P.; Eremets, M. I.; Troyan, I. A.; Ksenofontov, V.; Shylin, S. I. Conventional Superconductivity at 203 K at High Pressures in the Sulfur Hydride System. *Nature* **2015**, *525* (7567), 73−76.

(18) Goncharov, A. F.; Lobanov, S. S.; Kruglov, I.; Zhao, X.-M.; Chen, X.-J.; Oganov, A. R.; Konôpková, Z.; Prakapenka, V. B. Hydrogen Sulfide at High Pressure: Change in Stoichiometry. *Phys. Rev. B: Condens. Matter Mater. Phys.* **2016**, *93* (17), 174105.

(19) Esfahani, M. M. D.; Wang, Z.; Oganov, A. R.; Dong, H.; Zhu, Q.; Wang, S.; Rakitin, M. S.; Zhou, X.-F. Superconductivity of Novel Tin Hydrides (Sn_nH_m) under Pressure. *Sci. Rep.* **2016**, *6*, srep22873.

(20) Kruglov, I. A.; Kvashnin, A. G.; Goncharov, A. F.; Oganov, A. R.; Lobanov, S.; Holtgrewe, N.; Yanilkin, A. V. High-Temperature Superconductivity of Uranium Hydrides at near-Ambient Conditions. *arXiv:1708.05251* 2017, https://arxiv.org/abs/1708.05251.

(21) Davari Esfahani, M. M.; Oganov, A. R.; Niu, H.; Zhang, J. Superconductivity and Unexpected Chemistry of Germanium Hydrides under Pressure. *Phys. Rev. B: Condens. Matter Mater. Phys.* **2017**, *95* (13), 134506.

(22) Ma, Y.; Duan, D.; Shao, Z.; Yu, H.; Liu, H.; Tian, F.; Huang, X.; Li, D.; Liu, B.; Cui, T. Divergent Synthesis Routes and Superconductivity of Ternary Hydride $MgSiH_6$ at High Pressure. *Phys. Rev. B: Condens. Matter Mater. Phys.* **2017**, *96* (14), 144518.

(23) Kvashnin, A. G.; Semenok, D. V.; Kruglov, I. A.; Oganov, A. R. High-Temperature Superconductivity in Th-H System at Pressure Conditions. *arXiv:1711.00278* 2017, http://arxiv.org/abs/1711.00278.

(24) Drozdov, A. P.; Eremets, M. I.; Troyan, I. A. Superconductivity above 100 K in PH_3 at High Pressures. *arXiv:1508.06224* 2015, http://arxiv.org/abs/1508.06224.

(25) Kong, P. P.; Drozdov, A. P.; Eroke, E.; Eremets, M. I. Pressure-Induced Superconductivity above 79 K in Si_2H_6. In *Book of abstracts of AIRAPT 26 joint with ACHPR 8 & CHPC 19*; Biijing, China, 2017; p 347.

DOI: 10.1021/acs.jpcc.8b01270
J. Phys. Chem. C 2018, 122, 4731−4736

(26) Majumdar, A.; Tse, J. S.; Wu, M.; Yao, Y. Superconductivity in FeH_5. *Phys. Rev. B: Condens. Matter Mater. Phys.* **2017**, *96* (20), 201107.
(27) Cort, G.; Taylor, R. D.; Willis, J. O. Search for Magnetism in hcp ε-Fe. *J. Appl. Phys.* **1982**, *53* (3), 2064−2065.
(28) Shimizu, K.; Kimura, T.; Furomoto, S.; Takeda, K.; Kontani, K.; Onuki, Y.; Amaya, K. Superconductivity in the Non-Magnetic State of Iron under Pressure. *Nature* **2001**, *412* (6844), 316.
(29) Yadav, C. S.; Seyfarth, G.; Pedrazzini, P.; Wilhelm, H.; Černý, R.; Jaccard, D. Effect of Pressure Cycling on Iron: Signatures of an Electronic Instability and Unconventional Superconductivity. *Phys. Rev. B: Condens. Matter Mater. Phys.* **2013**, *88* (5), 054110.
(30) Kamihara, Y.; Watanabe, T.; Hirano, M.; Hosono, H. Iron-Based Layered Superconductor $La[O_{1-x}F_x]FeAs$ (x = 0.05−0.12) with T_C = 26 K. *J. Am. Chem. Soc.* **2008**, *130* (11), 3296−3297.
(31) Zhang, J.; Jiao, L.; Chen, Y.; Yuan, H. Universal Behavior of the Upper Critical Field in Iron-Based Superconductors. *Front. Phys.* **2011**, *6* (4), 463−473.
(32) Hosono, H.; Kuroki, K. Iron-Based Superconductors: Current Status of Materials and Pairing Mechanism. *Phys. C* **2015**, *514*, 399−422.
(33) Fernandes, R. M.; Chubukov, A. V.; Schmalian, J. What Drives Nematic Order in Iron-Based Superconductors? *Nat. Phys.* **2014**, *10* (2), 97.
(34) Eremin, I.; Knolle, J.; Fernandes, R. M.; Schmalian, J.; Chubukov, A. V. Antiferromagnetism in Iron-Based Superconductors: Selection of Magnetic Order and Quasiparticle Interference. *J. Phys. Soc. Jpn.* **2014**, *83* (6), 061015.
(35) Onari, S.; Kontani, H. Self-Consistent Vertex Correction Analysis for Iron-Based Superconductors: Mechanism of Coulomb Interaction-Driven Orbital Fluctuations. *Phys. Rev. Lett.* **2012**, *109* (13), 137001.
(36) Yamada, T.; Ishizuka, J.; Ono, Y. A High-Tc Mechanism of Iron Pnictide Superconductivity due to Cooperation of Ferro-Orbital and Antiferromagnetic Fluctuations. *J. Phys. Soc. Jpn.* **2014**, *83* (4), 043704.
(37) Oganov, A. R.; Ma, Y.; Lyakhov, A. O.; Valle, M.; Gatti, C. Evolutionary Crystal Structure Prediction as a Method for the Discovery of Minerals and Materials. Rev Miner. *Rev. Mineral. Geochem.* **2010**, *71*, 271.
(38) Lyakhov, A. O.; Oganov, A. R.; Stokes, H. T.; Zhu, Q. New Developments in Evolutionary Structure Prediction Algorithm USPEX. *Comput. Phys. Commun.* **2013**, *184*, 1172−1182.
(39) Oganov, A. R.; Glass, C. W. Crystal Structure Prediction Using Ab Initio Evolutionary Techniques: Principles and Applications. *J. Chem. Phys.* **2006**, *124*, 244704.
(40) Oganov, A. R.; Lyakhov, A. O.; Valle, M. How Evolutionary Crystal Structure Prediction Works—and Why. *Acc. Chem. Res.* **2011**, *44*, 227−237.
(41) Hohenberg, P.; Kohn, W. Inhomogeneous Electron Gas. *Phys. Rev.* **1964**, *136* (3B), B864−B871.
(42) Kohn, W.; Sham, L. J. Self-Consistent Equations Including Exchange and Correlation Effects. *Phys. Rev.* **1965**, *140* (4), A1133−A1138.
(43) Perdew, J. P.; Burke, K.; Ernzerhof, M. Generalized Gradient Approximation Made Simple. *Phys. Rev. Lett.* **1996**, *77* (18), 3865−3868.
(44) Blöchl, P. E. Projector Augmented-Wave Method. *Phys. Rev. B: Condens. Matter Mater. Phys.* **1994**, *50* (24), 17953−17979.
(45) Kresse, G.; Joubert, D. From Ultrasoft Pseudopotentials to the Projector Augmented-Wave Method. *Phys. Rev. B: Condens. Matter Mater. Phys.* **1999**, *59* (3), 1758−1775.
(46) Kresse, G.; Furthmüller, J. Efficient Iterative Schemes for Ab Initio Total-Energy Calculations Using a Plane-Wave Basis Set. *Phys. Rev. B: Condens. Matter Mater. Phys.* **1996**, *54*, 11169−11186.
(47) Kresse, G.; Hafner, J. Ab Initio Molecular Dynamics for Liquid Metals. *Phys. Rev. B: Condens. Matter Mater. Phys.* **1993**, *47*, 558−561.
(48) Kresse, G.; Hafner, J. Ab Initio Molecular-Dynamics Simulation of the Liquid-Metal Amorphous-Semiconductor Transition in Germanium. *Phys. Rev. B: Condens. Matter Mater. Phys.* **1994**, *49*, 14251−14269.
(49) Saxena, S. K.; Dubrovinsky, L. S.; Häggkvist, P.; Cerenius, Y.; Shen, G.; Mao, H. K. Synchrotron X-Ray Study of Iron at High Pressure and Temperature. *Science* **1995**, *269* (5231), 1703−1704.
(50) Belonoshko, A. B.; Ahuja, R.; Johansson, B. Stability of the Body-Centred-Cubic Phase of Iron in the Earth's Inner Core. *Nature* **2003**, *424* (6952), 1032−1034.
(51) Tateno, S.; Hirose, K.; Ohishi, Y.; Tatsumi, Y. The Structure of Iron in Earth's Inner Core. *Science* **2010**, *330* (6002), 359−361.
(52) Pickard, C. J.; Needs, R. J. Structure of Phase III of Solid Hydrogen. *Nat. Phys.* **2007**, *3* (7), 473−476.
(53) Giannozzi, P.; Baroni, S.; Bonini, N.; Calandra, M.; Car, R.; Cavazzoni, C.; Ceresoli, D.; Chiarotti, G. L.; Cococcioni, M.; Dabo, I.; et al. QUANTUM ESPRESSO: A Modular and Open-Source Software Project for Quantum Simulations of Materials. *J. Phys.: Condens. Matter* **2009**, *21*, 395502.
(54) Baroni, S.; de Gironcoli, S.; Dal Corso, A.; Giannozzi, P. Phonons and Related Crystal Properties from Density-Functional Perturbation Theory. *Rev. Mod. Phys.* **2001**, *73* (2), 515−562.
(55) Togo, A.; Tanaka, I. First Principles Phonon Calculations in Materials Science. *Scr. Mater.* **2015**, *108*, 1−5.
(56) Togo, A.; Oba, F.; Tanaka, I. First-Principles Calculations of the Ferroelastic Transition between Rutile-Type and $CaCl_2$-Type SiO_2 at High Pressures. *Phys. Rev. B: Condens. Matter Mater. Phys.* **2008**, *78*, 134106.
(57) Allen, P. B.; Dynes, R. C. Transition Temperature of Strong-Coupled Superconductors Reanalyzed. *Phys. Rev. B* **1975**, *12* (3), 905−922.
(58) Veblen, D. R. Polysomatism and Polysomatic Series: A Review and Applications. *Am. Minaralogist* **1991**, *76*, 801−826.
(59) Momma, K.; Izumi, F. VESTA 3 for Three-Dimensional Visualization of Crystal, Volumetric and Morphology Data. *J. Appl. Crystallogr.* **2011**, *44*, 1272−1276.
(60) Zhang, W.; Oganov, A. R.; Goncharov, A. F.; Zhu, Q.; Boulfelfel, S. E.; Lyakhov, A. O.; Somayazulu, M.; Prakapenka, V. B. Unexpected Stable Stoichiometries of Sodium Chlorides. *Science* **2013**, *342* (6165), 1502−1505.

DOI: 10.1021/acs.jpcc.8b01270
J. Phys. Chem. C 2018, 122, 4731−4736